Trajectory and Speed Control of Tracked Mobile Robot with Interval Type-2 TSK Fuzzy Logic Controller

Osman DOĞMUŞ*, Mahit GÜNEŞ

Kahramanmaraş Sütçü İmam University, 251/A Avşar Yerleşkesi Batı Çevreyolu Boulevard, Kahramanmaraş, 46050, Turkey
odogmus@ksu.edu.tr (*Corresponding author*), mgunes@ksu.edu.tr

Abstract: Multi-purpose mobile robots are used as models in the development of autonomous systems. They can also be used in multiple tasks, such as carrying materials to various environments, making measurements in hazardous areas, and performing specific operations such as reconnaissance and surveillance. Different control techniques are used in the speed and trajectory control of mobile robots. In this study, the trajectory and speed control of a tracked mobile robot (TMR) was carried out using an interval Type2 Takagi Sugeno Kang fuzzy logic controller (IT2TSKFLC). Simulation studies of the proposed control system were carried out in the Matlab/Simulink environment. The performance of the proposed IT2TSKFLC in speed and trajectory control of the mobile robot was compared with those of the classical PI controller and Type1 fuzzy logic controller (T1FLC). It has been demonstrated, through simulation studies, that IT2TSKFLC increases system performance and provides a more stable structure.

Keywords: Tracked mobile robot, Type1 FLC, Interval Type2 TSK FLC, PI.

1. Introduction

Tracked mobile robots are robots that can be operated in difficult terrain conditions and perform tasks that may be dangerous for people. They can be controlled remotely, and they have high maneuverability. These robots are used for applications such as search, rescue, and disposal of any bomb (Dian et al., 2019; Dong & Luo, 2011). Precise speed and trajectory control are very important for tracked mobile robots. Precise guidance of mobile robots to the desired position is needed for basic operation. In addition, robots often operate in complex environmental conditions. These environmental conditions directly affect the stability of the propulsion system. For this reason, the proposed control system should have the ability to reduce the effects of disturbances to meet the desired performance (Jayakumar & Kumar, 2012).

Today, PID controllers are still widely used in the control of mobile robots and industrial systems (Ben Jabeur & Seddik, 2021). However, since PID controllers have fixed parameters, they show poor performance in the control of systems with nonlinear and time-varying parameters (Blasko & Kaura, 1997). PID controllers need a complex mathematical model of the system to control speed, torque and position.

Recently, controller structures using artificial intelligence-based fuzzy logic, artificial neural networks, neural-fuzzy logic methods have been developed to minimize the undesirable features of traditional control approaches (Eltamaly, Alolah & Badr, 2010). These smart controllers are used successfully in a lot of industrial fields. One of these controllers is the T1FLC developed by Lotfi A. Zadeh (Zadeh, 1975). Fuzzy logic is defined as a set of rules that can be utilized for describe the action of complex systems which cannot be described mathematically (Kılıc, Ozcalık & Sit, 2018). T1FLC has been a great research focus because of its well performance against uncertain and nonlinear systems. On the other hand, T1FLC has some limitations such as poor performance in systems with high uncertainties and nonlinearities. Because of these problems, Zadeh (1975) has proposed the concept of Type2 Fuzzy Logic Controller (T2FLC), which is a generalized form of ordinary fuzzy sets (FS). The key feature of T2FLCs is the Uncertainty Footprint (FOU) (Lin, Chen & Lin, 2020), which identifies uncertainties and nonlinearities. So, in T2FLCs, the values of the membership function (MFs) of each element are not exact as in T1FLC, but they consist of a three-dimensional FS. Many studies have shown that T2FLC is much more successful at dealing with uncertainties and nonlinearities than T1FLC (Abdelmoaty, Canbek & Oniz, 2022).

Pour, Alsayegh & Jaradat (2022) examined the impact of an adaptive PID controller with type2 fuzzy on the mobile robot. The recommended adaptable controller's PID parameters are automatically adjusted using type2 fuzzy systems. Asai, Chen & Takami (2019) used a neural network controller structure that is PD-like for the TMR to follow a trajectory. Recommended online neural network checker, it has the features of self-training and PD control-like feedback structure. Ji

et al. (2018) stated that, in a TMR directed with two DC motors, factors such as load distortion and mechanical structure difference between right track and left track affect tracking accuracy and give rise to trajectory tracking error. To solve these problems, they suggested a cross-coupled sliding cloud-model controller. Sidi et al. (2018) presented the speed control of a TMR modeling with three degrees of freedom with PID in a Matlab/Simulink environment. Huang et al. (2018) introduced a PI-type trajectory tracking controller based on forward point information with a navigation system for a differentially driven TMR. Ye, Yao & Yang (2016) proposed a second-order linear active decay rejection control (LADRC) as disturbance isolation so that the mobile robot system can consistently and accurately follow the set speed. LADRC is expected to estimate the disruptive effects that affect the system without depending on the system model. The proposed control system is compared by the PID controller. Bae, Lee & Cho (2020) presented a sensor and sensorless type of autonomous robot with two in-wheel brushless DC motors to control the driving speed and direction of motion. The current model used the estimation method of sensorless with model reference adaptable system based, on continuous velocity feedback. Peng et al. (2020) suggested a new active disturbance rejection control (ADRC) method for the problem of coordinated motion and speed control of the steering and driving robot with four wheel-legs with inner modeling ambiguity and outer noise. It combined the routing model with the ADRC consensus protocol to solve the consensus problem when routing the robot. Najmurrokhman et al. (2019) designed and implemented the obstacle avoidance and speed control of a hexapod robot, which resembles an insect, using a Mamdani-type FLC. The proposed controller can effectively track a desired trajectory with minimum tracking error, even under in case of dynamic load conditions and sudden speed change. The output of the offered controller is smoother than those of the others. This reduces motor wear and saves energy.

The remainder of the paper is organized as follows: Section 2 analyses the analytical TMR's dynamic and kinematic mathematical models. It also explains the Matlab/Simulink design of these models. Section 3 describes the structure of the IT2TSKFLC Design. Section 4 mentions the simulation studies and interpretation of the graphs obtained. Section 5 presents some results and concluding remarks.

2. TMR Design and Mathematical Model

In this section, the physical parameters of the TMR, the design of analytical TMR's kinematic and dynamic mathematical models, and the Matlab/Simulink design of TMR with the mathematical models obtained are described.

2.1 TMR Design

For the construction of the mechanical parts of the designed differential steered TMR, two 120 W brushed DC motors, rolling bearings for the motor and wheel shafts, an 8 mm aluminum plate in 45 x 65 cm size, steel and aluminum gears, and two bidirectional 1440 mm timing belts were used. The three-dimensional design of TMR is shown in Figure 1. The real design of the TMR is shown in Figure 2.
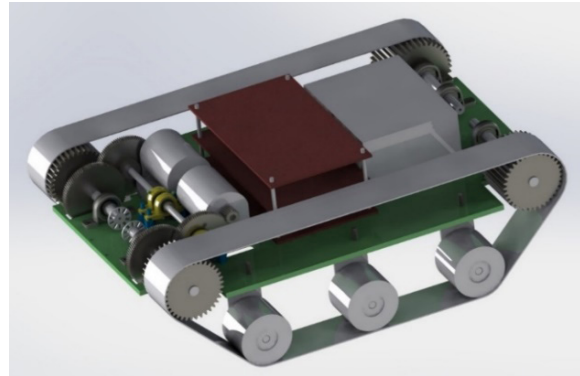

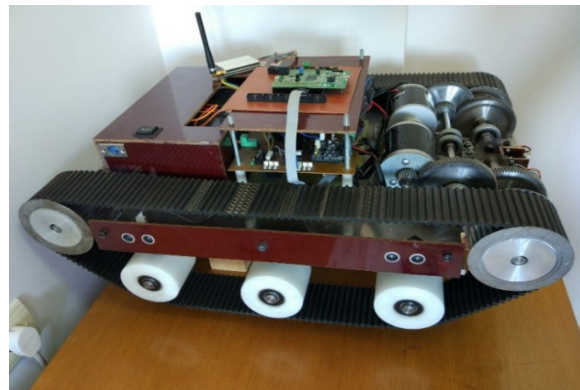**Figure 1.** Three-dimensional model of the TMR

Figure 2. Visual of the TMR

The physical parameters of the TMR, which will be utilized in the simulation models, are shown in Table 1. The parameters of the DC motors used in the TMR are indicated in Table 2.

The moment of inertia in Table 1 was calculated in equation 1 (Serway et al., 2016):

$$J_z = \frac{m}{12}\left(d^2 + \ell^2\right) \tag{1}$$

where L_a, R_a, K_b, K_t, and b parameters were determined according to the results of motor tests. (Malu & Majumdar, 2014).

Table 1. Measured physical parameters of the TMR

Symbol	Quantity	Value
m	Total vehicle mass	36,37 kg
d	Distance between the TMR center and tracks	45 cm
ℓ	Body length	65 cm
r	Radius of sprocket	45,8 mm
N_g	Gear ratio of gearbox	14,78
v_a	Maximum vehicle speed	1,15 m/s
J_Z	Z-axis moment of inertia	1,875 kgm²

Table 2. Parameters of the DC motor

Symbol	Quantity	Value
P	Power	120 W
n	Speed	2750 rpm
T_m	Torque	0,42 Nm
U_a	Armature Voltage	24 V
I_a	Armature Current	5 A
L_a	Armature Inductance	1,59 mH
R_a	Armature Resistance	1,137 Ω
K_b	Back-emf constant	0,06467 Nm/A
K_t	Torque constant	0,06467 Nm/A
b	Viscous friction coefficient	98,8×10⁻⁶ Nm/s

The differential equation of the electrical part of the DC motor required for the mathematical model is defined as follows (Vidlak, Makys, & Stano, 2021):

$$\frac{dI_a}{dt} = \frac{1}{L_a} U_a - \frac{R_a}{L_a} I_a - \frac{K_b}{L_a} w_m \quad (2)$$

where w_m is the rotor angular velocity. The power is transferred to the tracks using a gearbox. The angular velocity of the track sprocket is determined in equation 3:

$$w_g = \frac{w_m}{N_g} \quad (3)$$

2.2 TMR Kinematic Analytical Model

To generate a kinematic model, the view of the TMR in the coordinate plane is shown in Figure 3. Mathematical expressions are given in equations 4-9 (Huang et al., 2018; Gholipour & Yazdanpanah, 2003).

$$v_R = r w_{gR}, v_L = r w_{gL} \quad (4)$$

$$v_a = \frac{v_R + v_L}{2} \quad (5)$$

$$w_o = \frac{v_R - v_L}{d} \quad (6)$$

$$\dot{x} = v_a \cos\psi \quad (7)$$

$$\dot{y} = v_a \sin\psi \quad (8)$$

$$\dot{\psi} = w_o \quad (9)$$

where r is the radius of the track sprocket; w_{gL} and w_{gR} are the angular velocity of the left and right track sprocket, respectively; w_o is the angular velocity; d is the distance between the TMR center and tracks; v_R and v_L right and left tracks speeds, respectively; v_a is the linear speed of the TMR; ψ is the angle according to the x-axis; $v_a \cos\psi$ and $v_a \sin\psi$ are the components of v_a along its X and Y axes.
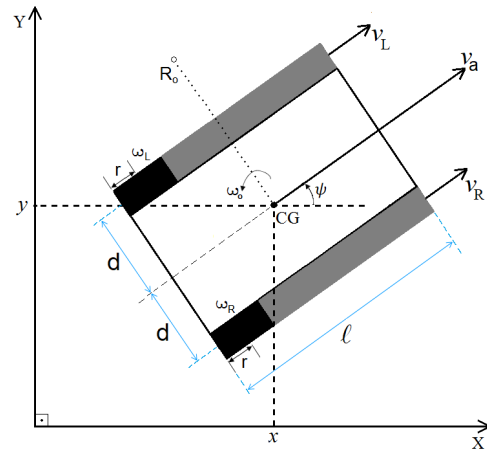

Figure 3. Kinematic model

2.3 TMR Dynamic Analytical Model

The dynamic model of the mobile robot was extracted by making use of its appearance on the coordinate plane shown in Figure 4, and the mathematical expressions are given in equations 10-17 (Ayedi, Boujelben & Rekik, 2018; Wu, Xu & Wang, 2013).
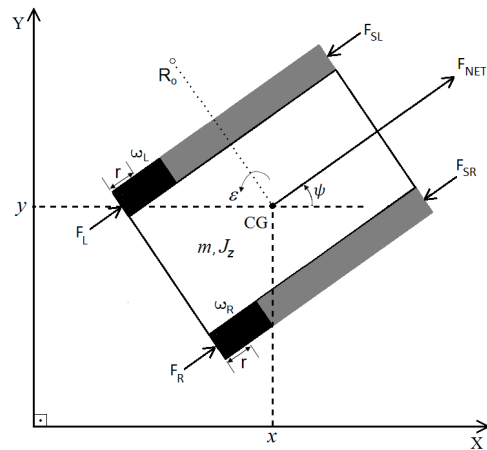

Figure 4. Dynamic model

$$ma = F_T - F_S \tag{10}$$

$$m\frac{dv_a}{dt} = (F_R + F_L) - F_S \tag{11}$$

$$J_Z\varepsilon = M_T - M_S \tag{12}$$

$$J_Z\frac{dw_o}{dt} = (F_R - F_L)\frac{d}{2} - M_S \tag{13}$$

$$F_R = \frac{M_R}{r}, \; F_L = \frac{M_L}{r} \tag{14}$$

$$M_R = N_g M_{mR}, \; M_L = N_g M_{mL} \tag{15}$$

$$M_{mR} = K_t I_R, \; M_{mL} = K_t I_L \tag{16}$$

$$F_R = \frac{N_g K_t}{r} I_R, \; F_L = \frac{N_g K_t}{r} I_L \tag{17}$$

where m and a are mass and acceleration of the TMR, respectively; F_R and F_L are right and left force of track sprockets, respectively; F_T and F_S are total and friction forces, respectively; J_Z is inertia moment of the TMR; ε is the angular rotational acceleration; M_R and M_L are moments of right and left track sprockets, respectively; M_{mR} and M_{mL} are moments of right and left rotors, respectively; M_T and M_S are total and friction moments, respectively; N_g is gear conversion ratio; K_t is DC motor torque constant; I_R and I_L represent right and left motor currents, respectively.

The state vector of the control system is given in equation 18 and the input vector of the control system is given in equation 19:

$$q = \begin{bmatrix} v_a & w_o & I_L & I_R \end{bmatrix}^T \tag{18}$$

$$u = \begin{bmatrix} F_S & M_S & U_L & U_R \end{bmatrix}^T \tag{19}$$

The differential equations 20-21 depending on v_a and w_o variables in the state vector were obtained by using equations 2-6.

$$\dot{v}_a = \frac{N_g K_t}{mr} I_L + \frac{N_g K_t}{mr} I_R - \frac{1}{m} F_S \tag{20}$$

$$\dot{w}_o = -\frac{N_g K_t d}{J_Z r} I_L + \frac{N_g K_t d}{J_Z r} I_R - \frac{1}{J_Z} M_S \tag{21}$$

Likewise, I_L and I_R variables in equations 22-23 were obtained by using equations 10-17.

$$\dot{I}_L = -\frac{N_g K_b}{L_a r} v_a + \frac{N_g K_b d}{L_a r} w_o - \frac{R_a}{L_a} I_L + \frac{1}{L_a} U_L \tag{22}$$

$$\dot{I}_R = -\frac{N_g K_b}{L_a r} v_a - \frac{N_g K_b d}{L_a r} w_o - \frac{R_a}{L_a} I_R + \frac{1}{L_a} U_R \tag{23}$$

The state space form of the dynamic model of TMR is given in equation 24-29.

$$\dot{q} = Aq + Bu \tag{24}$$

$$y = Cq + Du \tag{25}$$

where y is output vector of the control system.

$$A = \begin{bmatrix} 0 & 0 & \dfrac{N_g K_t}{mr} & \dfrac{N_g K_t}{mr} \\ 0 & 0 & -\dfrac{N_g K_t d}{Jr} & \dfrac{N_g K_t d}{Jr} \\ -\dfrac{N_g K_b}{L_a r} & \dfrac{N_g K_b d}{L_a r} & -\dfrac{R_a}{L_a} & 0 \\ -\dfrac{N_g K_b}{L_a r} & -\dfrac{N_g K_b d}{L_a r} & 0 & -\dfrac{R_a}{L_a} \end{bmatrix} \tag{26}$$

$$B = \begin{bmatrix} -\dfrac{1}{m} & 0 & 0 & 0 \\ 0 & -\dfrac{1}{J_Z} & 0 & 0 \\ 0 & 0 & \dfrac{1}{L_a} & 0 \\ 0 & 0 & 0 & \dfrac{1}{L_a} \end{bmatrix} \tag{27}$$

$$C = \begin{bmatrix} 1 & 0 & 0 & 0 \\ 0 & 1 & 0 & 0 \\ 0 & 0 & 1 & 0 \\ 0 & 0 & 0 & 1 \end{bmatrix} \tag{28}$$

$$D = [0] \tag{29}$$

2.4 Creating the Matlab/ Simulink Model

The Matlab/Simulink model of the mobile robot is illustrated in Figure 5.
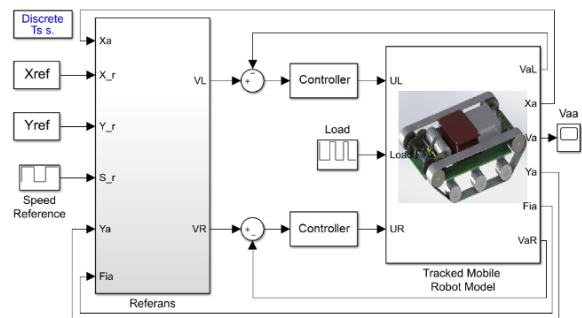

Figure 5. Matlab/Simulink model of the system

Figure 6 represents the internal structure of the calculation block. In this block diagram, using the reference position and reference speed information, position and rotation angle errors, reference left and right pallet velocities are calculated with inverse tangent transformations.

The model of the TMR is composed of two parts, the Dynamic and the Kinematic block diagrams, as shown in Figure 7. The dynamic model seen in Figure 8 was created using equations 20-23. The kinematic model seen in Figure 9 was created using equations 4-9.
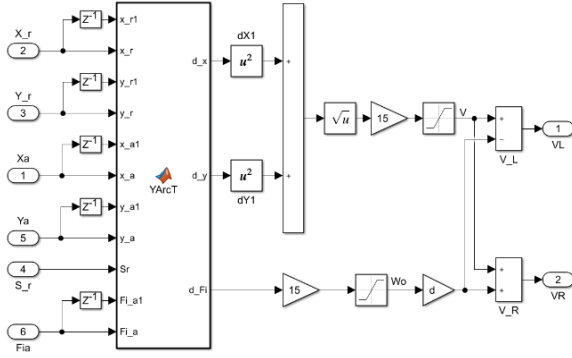

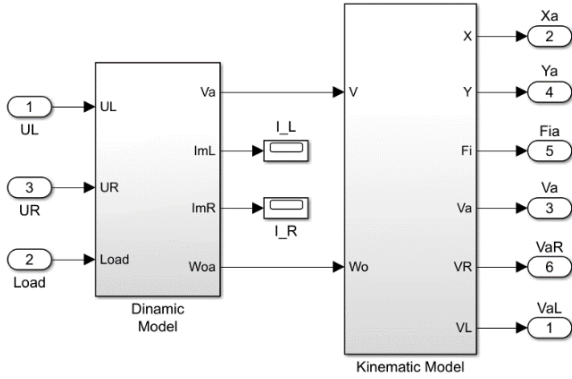**Figure 6.** Computational block internal structure

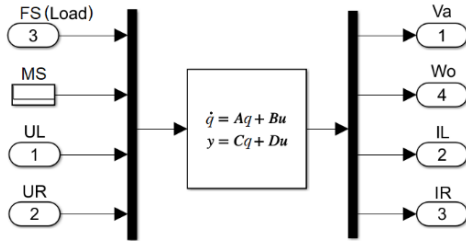**Figure 7.** Internal block diagram of the TMR model

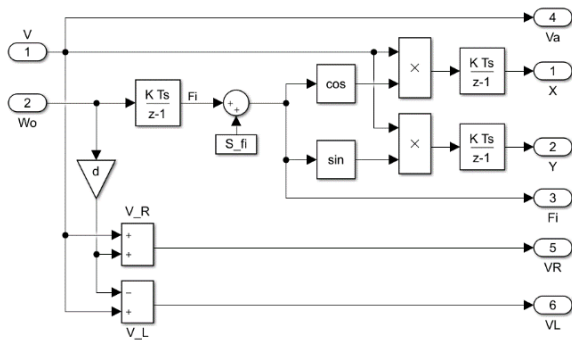**Figure 8.** Dynamic model of TMR

Figure 9. Kinematic model of TMR

3. Interval Type-2 TSK FLC Design

In this part, Interval Type-2 Sets (IT2S) and the structure of the general IT2FLC and designed IT2FLC's features are explained.

3.1 Interval Type-2 Fuzzy Sets

According to Lotfi A. Zadeh's theory (1975), T2FS is an extension of T1FS. The main difference between them is that while the MF in T1FS is a net number, the MF in T2FS is a FS (Mallick & Das, 2023). The FS of the general T2FS can be expressed by equation 30:

$$\tilde{A} = \left\{ \left((x,u), \mu_{\tilde{A}}(x,u) \right) \mid \forall x \in X, \right.$$
$$\left. \forall u \in [0,1], \ \mu_{\tilde{A}} \in [0,1] \right\} \tag{30}$$

where x is the input value of the FS; u is the primary membership value; $\mu_{\tilde{A}}$ is the secondary membership value; $\tilde{A}$ is a set with a three-dimensional structure and $\mu_{\tilde{A}}(x,u)$ has a value within the range [0, 1] in general T2FS. Intervals T2FSs (IT2FS) are presented as an alternative to alleviate mathematical calculation load (Coteli et al., 2017). As it can be seen in Figure 10, in IT2FLS, it is taken as $\mu_{\tilde{A}}(x,u) = 1$. In this case, the set $\tilde{A}$ in IT2FLS can be defined in equation 31:

$$\tilde{A} = \left\{ \left((x,u), 1 \right) \mid \forall x \in X, \ \forall u \in [0,1] \right\} \tag{31}$$

where u is a value within the range $\left[\overline{\mu}(x'), \underline{\mu}(x') \right]$ corresponding to the input x'.
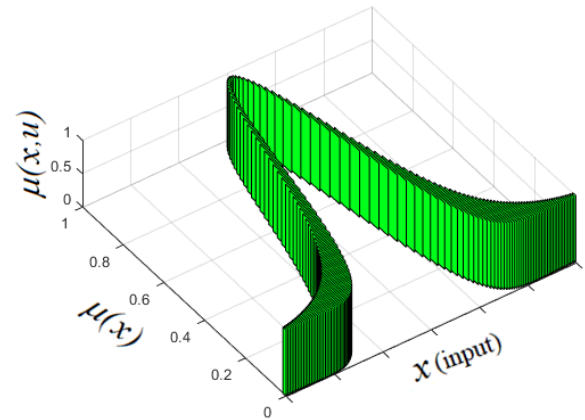

Figure 10. Three-dimensional Gaussian of IT2FS

$\overline{\mu}(x')$ and $\underline{\mu}(x')$ are a T1FS, the upper MF (UMF) and the lower MF (LMF), respectively. The uncertainty footprint (FOU) shown in Figure 11 is the bounded area representing the primary

ambiguity of the T2FS between the UMF and LMF. As it can be seen from Figure 11, the location of u cannot be determined exactly. It is assumed that the FOU domain is an infinite Type-1 MF (Karnik & Mendel, 1998).
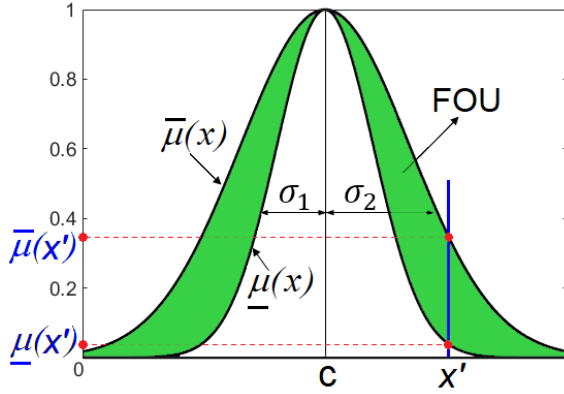

Figure 11. Gaussian of IT2FS

3.2 Interval Type-2 FLC

In T1FLC, the membership degree of T1FSs is a single value between [0, 1]. When a system has a large amount of uncertainty, T1FLCs may not reach the desired performance level with the reasonable complexity of the structure (Mendel & John, 2002). These uncertainties may include kinematic and dynamic model uncertainty of the system, external disturbances from the unknown environment, distorted reference trajectories, and noise (Sun et al., 2019).

In T2FLC, the membership degrees of T2FSs are fuzzy values between UMF and LMF. Thus, uncertainties in the system are made expressible.

The most important difference between IT2FLC and T1FLC is the type reduction method. T2FSs can be transformed into T1FSs by the type reduction method. The output of the type reduction block corresponds to the T1FS (Antão, 2017). The comprehensive structure of IT2TSKFLC is shown in Figure 12. As shown in Figure 12, crisp inputs are fuzzified with Type-2 input MFs. After this process, the Type-2 fuzzy output set is created according to the input sets, membership degree, and fuzzy rule base. Crisp values of IT2TSKFLC were obtained after type reduction and fuzzification processes (Takagi & Sugeno, 1985). The proposed IT2TSKFLC inference method has been defined in three different models: A2C1, A2C0, and A1C1.
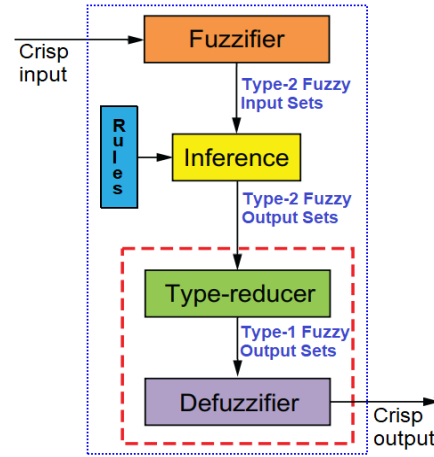

Figure 12. Block diagram of the IT2TSKFLC

In this study, the A2C0TSK model has been used as the inference method of IT2TSKFLC. While the inputs of the reduction block are T2FSs, the outputs are first-order polynomials in the A2C0TSK model.

A2C0TSK model structure can be specified with If-Then fuzzy rules, as in equation 32 (Liang & Mendel, 2000):

$$R^k : IF\ x_1\ is\ \tilde{A}_1^j\ AND\ x_2\ is\ \tilde{A}_2^j\ THEN$$
$$LF_k = p_k x_1 + q_k x_2 + r_k \tag{32}$$

where R^k represents the kth fuzzy rule; {k =1,2, ...,K} where K is the number of fuzzy rule; x_1 and x_2 are input variables; $\tilde{A}_1^j$ and $\tilde{A}_2^j$ are MFs; {j=1,2,...,J} where J is the number of MF; LF_k is linear output of rule; p_k, q_k, r_k denote the consequent polynomial parameters.

Although various types of curves are used in the specialized literature, the most commonly used in fuzzification is Gaussian MF (Kayacan & Khanesar, 2015). The reason for using Gaussian MF is that there is no roughness in any of the points of the control algorithm and it does not reach the zero point. The result of using the Gaussian function will also affect the power stabilization for stationary systems (Wu, 2012).

The equations of Gaussian MF are given in equations 33-34, respectively:

$$\overline{\mu}_{\tilde{A}_i^j}(x_i) = exp\left\{-\frac{1}{2}\left(\frac{x_i - c_{ij}}{\overline{\sigma}_{ij}}\right)^2\right\} \tag{33}$$

$$\underline{\mu}_{\tilde{A}_i^j}(x_i) = exp\left\{-\frac{1}{2}\left(\frac{x_i - c_{ij}}{\underline{\sigma}_{ij}}\right)^2\right\} \tag{34}$$

where $i=1,2$ is the number of inputs; $j=1,2,...,5$ is the MF number; x_i is the input values; c_{ij} is the center of Gaussian function; σ_{ij} is the width of Gaussian function; and $\mu_{\tilde{A}_i^j}(x_i)$ represents the membership degrees for the input variables (Kececioglu et al., 2019).

3.3 Design Features of IT2FLC

The configuration of IT2TSKFLC consists of 8 layers, as shown in Figure 13.

Layer-1: This layer is the input layer. Here the input variables of IT2TSKFLC are defined. The input variables are error (e) and change in error (Δe).

$$x_1 = e \qquad (35)$$

$$x_2 = \Delta e \qquad (36)$$

Layer-2: In this layer, membership degrees are calculated for each input. Each input is fuzzified with a five Gaussian MF, as in Figure 14. These FSs are positive big (PB), positive small (PS), zero (ZE), negative small (NS), and negative big (NB).

Layer-3: In this layer, the firing powers (f_k) of the rules are calculated. f_k is calculated by multiplying the membership values for each entry, as given in equations 37-38:

$$\overline{f_k} = \overline{\mu}_{\tilde{A}_1^j}(x_1) \cdot \overline{\mu}_{\tilde{A}_2^j}(x_2) \qquad (37)$$

$$\underline{f_k} = \underline{\mu}_{\tilde{A}_1^j}(x_1) \cdot \underline{\mu}_{\tilde{A}_2^j}(x_2) \qquad (38)$$

where $k = 1, 2, ..., 25$.

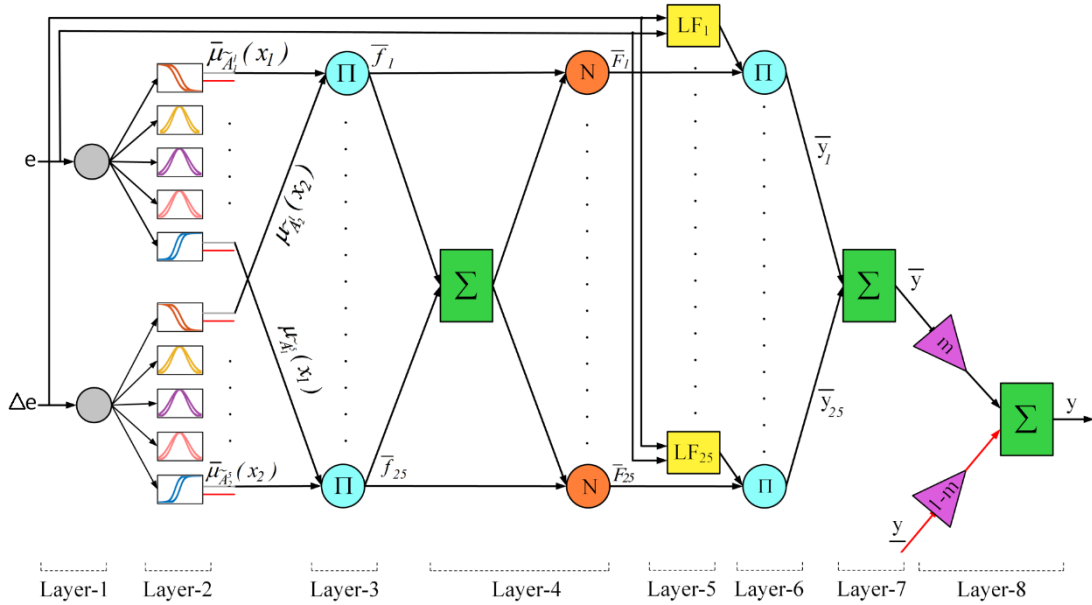The fuzzy rules of the used control structure are specified in Table 3.

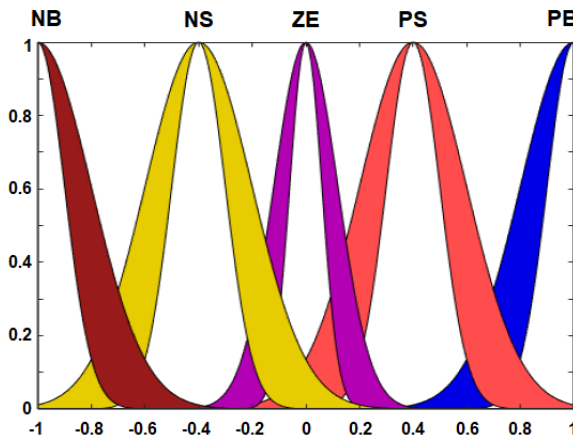

Figure 13. Structure of the IT2-TSK-FLC

Figure 14. Gaussian MFs

Table 3. Rule table for fuzzy inference system

e \ Δe	NB	NS	ZE	PS	PB
NB	LF_1	LF_2	LF_3	LF_4	LF_5
NS	LF_6	LF_7	LF_8	LF_9	LF_{10}
ZE	LF_{11}	LF_{12}	LF_{13}	LF_{14}	LF_{15}
PS	LF_{16}	LF_{17}	LF_{18}	LF_{19}	LF_{20}
PB	LF_{21}	LF_{22}	LF_{23}	LF_{24}	LF_{25}

Layer-4: This layer is the normalization layer and consists of nodes denoted by N. Firing powers (F_k), which represent the normalization process, are defined as the bottom and the top firing powers, respectively, as expressed in equations 39-40:

$$\overline{F_k} = \frac{\overline{f_k}}{\sum_{n=1}^{25} \overline{f_n}} \qquad (39)$$

$$\underline{F_k} = \frac{\underline{f_k}}{\sum_{n=1}^{25} \underline{f_n}} \qquad (40)$$

Layer-5: In this layer, the linear function (LF) outputs are calculated based on the rule base. The layer outputs are calculated as follows:

$$LF_k = p_k x_1 + q_k x_2 + r_k \qquad (41)$$

where p, q and r are the coefficients of LFs.

Layer-6: In this layer, the $\overline{y_k}$ and the $\underline{y_k}$ output signals are obtained by multiplying F_k, LF_k as seen in equations 42-43:

$$\overline{y_k} = \overline{F_k}.LF_k \qquad (42)$$

$$\underline{y_k} = \underline{F_k}.LF_k \qquad (43)$$

Layer-7: This layer collects the Layer-6 output signals and the lower and upper output signals are obtained:

$$\overline{y} = \sum_{k=1}^{25} \overline{y_k} \qquad (44)$$

$$\underline{y} = \sum_{k=1}^{25} \underline{y_k} \qquad (45)$$

Layer-8: This layer is the output layer of the controller where a reduction and clarification method using the Biglarbegian-Angel-Mendel method is performed. The output signal is obtained by summing the lower and upper output signals at certain rates, as expressed in equations 46-47:

$$y = (m).\overline{y} + (1-m).\underline{y} \qquad (46)$$

$$y = m \cdot \frac{\sum_{k=1}^{25} \overline{f_k}.LF_k}{\sum_{k=1}^{25} \overline{f_k}} + (1-m) \cdot \frac{\sum_{k=1}^{25} \underline{f_k}.LF_k}{\sum_{k=1}^{25} \underline{f_k}} \qquad (47)$$

where m is a value situated within the range [0-1] and it determines the effect ratio of the upper and lower output signals to the controller output signal.

4. Simulations and Results

The state space matrices A and B, which depend on the parameters given in Table 1 and Table 2, are expressed by equations 48-49.

$$A = \begin{bmatrix} 0 & 0 & 0,57 & 0,57 \\ 0 & 0 & -2,50 & 2,50 \\ -13114 & 2951 & -715 & 0 \\ -13114 & -2951 & 0 & -715 \end{bmatrix} \qquad (48)$$

$$B = \begin{bmatrix} -0,0275 & 0 & 0 & 0 \\ 0 & -0,533 & 0 & 0 \\ 0 & 0 & 628,93 & 0 \\ 0 & 0 & 0 & 628,93 \end{bmatrix} \qquad (49)$$

The LF coefficients of IT2TSKFLC were determined using the specialized literature as $p = [2\ 1.5\ 0.25\ 1.5\ 2]$, $q = [1\ 0.8\ 0.1\ 0.8\ 1]$ and $r = [0\ 0\ 0\ 0\ 0]$ (Kececioglu, 2022). The value of the m coefficient in the output layer is commonly considered to be 0.5 (Tavoosi et al., 2021).

A sinusoidal trajectory having a peak value of 3 m and a period of 10 m was used for the simulation of the designed TMR. The TMR follows the desired reference trajectory with 0.75 m/s between 0-10th seconds, 0.5 m/s between 10-20th seconds and 0.75 m/s speed between 20-25th seconds has been requested. Also, to measure the performance of the controllers against disruptive effects, a load of 6 kg was applied to the TMR when between 6-9th seconds and 13.5-16.5th seconds. Sampling time of simulation is 10 ms.

The success of following the created reference trajectory with determined constant speeds is shown in Figure 15. The trajectory tracking successes of all three controllers as x-axis and y-axis position errors are given in Figures 16-17.

The speed graph of the TMR obtained in these operating conditions is given in Figure 18. The extended appearance of the marked areas from Figure 18 is shown in Figure 19. The graph of the left motor control signs is given in Figure 20. Figure 21 illustrates the extended appearance of the marked areas from Figure 20. Since the slope of the sinusoidal orbit changes at every point (or continuously), the error rates of the controllers in tracking the orbit also vary according to the value of this slope. The x-axis position errors are greater at points where the slope changes too much (Figure 16). The biggest error, while following the reference trajectory, occurred at a speed of 0.75 m/s and at the peak of the trajectory. The biggest errors are 3.8 cm

for the PI controller, 2.85 cm for the T1FLC, and 2.65 cm for the IT2TSKFLC. The y-axis position errors are greater at zero crossing points of the sinus curve (Figure 17). The biggest error in the y-axis occurred at the moment of starting. The biggest errors are 4.0 cm for the PI controller, 2.6 cm for the T1FLC, and 2.44 cm for the IT2TSKFLC.
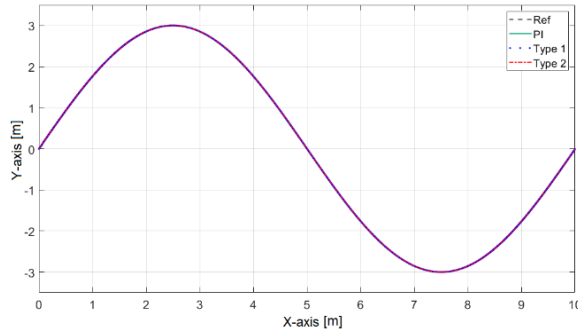

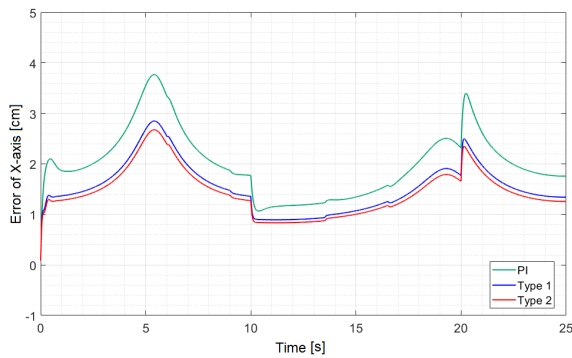**Figure 15.** Reference and TMR trajectories
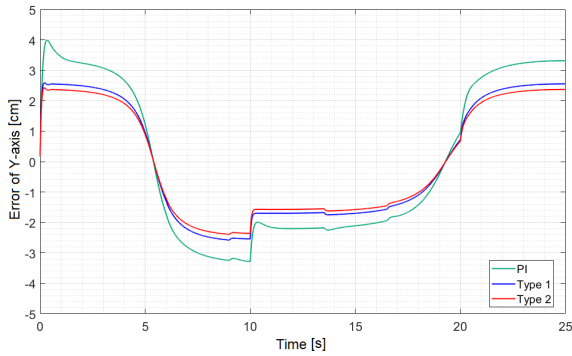

Figure 16. TMR position errors in x-axis

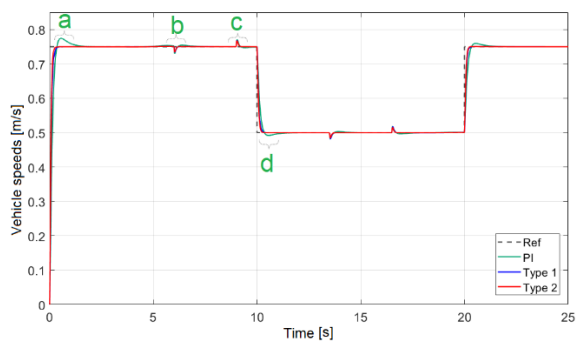**Figure 17.** TMR position errors in y-axis

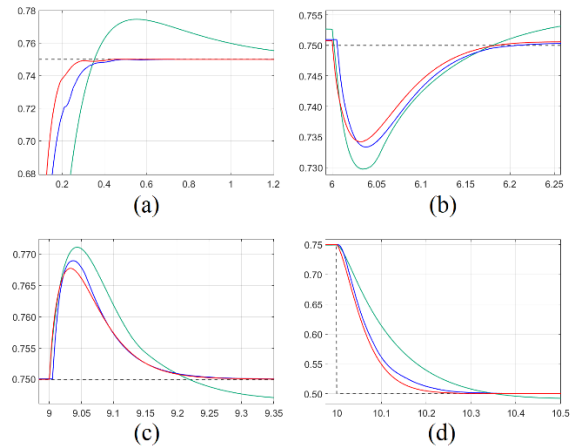**Figure 18.** Reference and TMR speeds

Figure 19. Enlarged appearance of the marked areas from Figure 18
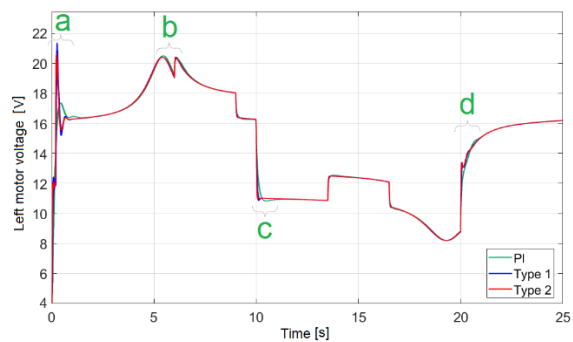
Figure 20. Control sign of the left motor voltage
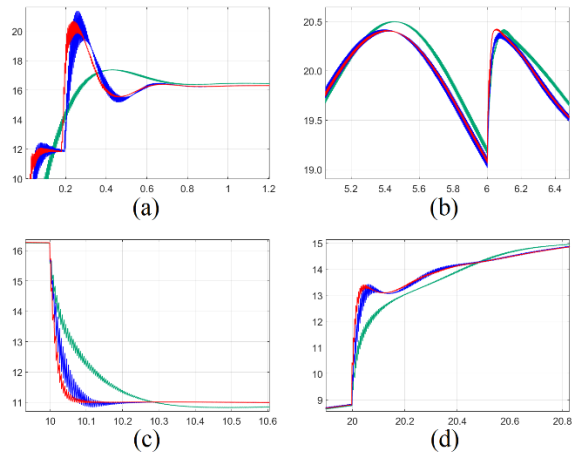
Figure 21. Enlarged appearance of the marked areas from Figure 20

The speed graphics of the three controllers are shown in Figure 18. The data in Table 4 explains point (a) of Figures 18-19. The settling times and overshoot values of the three controllers at different times are given in Table 5. The data in Table 5 explains points (b), (c), and (d) of Figures 18-19. As clearly shown in Figure 19 and Table 4, the performance of IT2TSKFLC is better than the ones of the T1FLC and the PI controller.

Table 4. Performance of controllers at startup

Controller	Rising Time (s)	Settling Time (s)	Peak Overshoot
IT2TSKFLC	0.107	0.30	0.00%
T1FLC	0.128	0.45	0.00%
PI	0.211	1.53	3.33%

Table 5. Performance of controllers under variable load and speed

	Controller	Settling Time (s)	Peak Overshoot
6th sec. (b)	IT2TSKFLC	0.18	2.10%
	T1FLC	0.20	2.23%
	PI	1.10	2.71%
9th sec. (c)	IT2TSKFLC	0.27	2.37%
	T1FLC	0.31	2.53%
	PI	0.90	2.82%
10th sec. (d)	IT2TSKFLC	0.28	0.00%
	T1FLC	0.34	0.00%
	PI	1.15	1.88%

Figure 20 indicates the output voltage graphics of the controllers. The enlarged view of points (a), (b), (c) and (d) in Figure 20 is shown in Figure 21. When the left motor control sign of the TMR from Figures 20-21 are examined, the voltage signal applied by the IT2TSKFLC to the motor is smoother than that of other controllers, that is, the fluctuation in the signal is less, as seen in Figure 21. At the same time, the IT2TSKFLC responded faster to disturbances or speed changes. At the 6th seconds, when a load of 6 kg is applied to the TMR, the controllers keep the speed constant by increasing the output voltage (Figure 20). At the 9th second, when the load is removed, the controllers reduce the output voltage to keep the speed constant.

Performance indices such as integral square error (ISE in equation 50) and mean absolute error (MAE in equation 51) were used to evaluate the effectiveness of the proposed controller in trajectory tracking and speed control.

$$ISE = \sum_{k=1}^{N} e^2 [k].T_s \tag{50}$$

$$MAE = \frac{1}{N}\sum_{i=1}^{N}|e[k]| \tag{51}$$

where $e[k]$ is the error at the kth time step; T_s is the sampling period; N is a total number of samples. The distance and speed errors are calculated as follows:

$$p_e^{\ k} = \sqrt{\left(x_r^{\ k} - x^k\right)^2 + \left(y_r^{\ k} - y^k\right)^2} \tag{52}$$

$$v_e^{\ k} = v_r^{\ k} - v^k \tag{53}$$

where p_e is the position error; x_r and y_r are the points of reference trajectory; x and y are the points of TMR trajectory; v_e is the speed error; v_r is the reference speed; v is the speed of TMR.

Performance indices for the three controllers are shown in Table 6.

Table 6. Comparison of controllers

	Trajectory		Speed	
Controller	ISE	MAE	ISE	MAE
IT2TSKFLC	0.0014	0.0022	0.027	0.0036
T1FLC	0.0016	0.0025	0.031	0.0042
PI	0.0028	0.0033	0.047	0.0075

5. Conclusion

In this study, a system model of a real TMR was obtained and a desired constant speed and trajectory control were performed using the IT2TSKFLC. The performance of the controller used in the present paper was compared with that of T1FLC and of classical PI controller.

TMR speed control results were observed using three different control methods, as shown in the simulation result.

The rising time value of the speed parameter of TMR was 0.211 s in the PI controller, while, in the T1FLC, this value was measured as 0.128 s. The rising time was found to be 0.107 s in the IT2TSKFLC.

In IT2TSKFLC, the settling time entered the steady-state 0.15 s earlier compared to T1FLC, with a settling time of 0.3 s. IT2TSKFLC entered earlier by 1.23 s compared to PI controller, resulting in a shorter duration for the unwanted transient response. While the maximum overshoot was %0 in T1FLC and IT2TSKFLC, it was measured as %3.33 in the PI controller.

The control system used for the three methods was compared with the disturbance effect. As a result of the comparison, the settling times of the three methods were examined and it was demonstrated that IT2TSKFLC became stable in 0.18 s, T1FLC in 0.20 s and PI controller in 1.10 s, respectively.

According to the performance indices, it becomes clear that ISE and MAE are minimum for the IT2TSKFLC. By examining all the

operating situations, it can be clearly noticed that IT2TSKFLC is more successful than T1FLC and PI controller. It has been seen that the IT2TSKFLC type controller is successful for constant speed and trajectory control of tracked robots with a complex model in a simulation platform.

IT2TSKFLCs are predicted to be used in the applications of real TMR.

REFERENCES

Abdelmoaty, O. K. H., Canbek, K. O. & Oniz, Y. (2022) Target Search and Tracking with an Autonomous Quadcopter using Type-2 Fuzzy Logic Controller. In: *Innovations in Intelligent Systems and Applications Conference (ASYU), 07-09 September 2022, Antalya, Turkey.* New Jersey, U.S.A., Institute of Electrical and Electronics Engineers (IEEE). pp. 1-6. doi: 10.1109/ASYU56188.2022.9925291.

Antão, R. (2017) *Type-2 Fuzzy Logic Uncertain Systems' Modeling and Control.* Singapore, Springer Nature Singapore. doi: 10.1007/978-981-10-4633-9.

Asai, M., Chen G. & Takami, I. (2019) Neural network trajectory tracking of tracked mobile robot. In: *16th International Multi-Conference on Systems, Signals and Devices (SSD), 21-24 March 2019, Istanbul, Turkey.* New Jersey, U.S.A., Institute of Electrical and Electronics Engineers (IEEE). pp. 225–230. doi: 10.1109/SSD.2019.8893152.

Ayedi, D., Boujelben, M. & Rekik, C. (2018) Hybrid Type-2 Fuzzy-Sliding Mode Controller for Navigation of Mobile Robot in an Environment Containing a Dynamic Target. *Journal of Robotics.* 2018, 1-10. doi: 10.1155/2018/ 8421848.

Bae, J., Lee, D.-H. & Cho, K. (2020) Speed and Direction Control of Two In-wheel BLDC Motors for the Self-Driving Surveillance Robot. In: *2020 6th International Conference on Mechatronics and Robotics Engineering (ICMRE), 12-15 February 2020, Barcelona, Spain.* New Jersey, U.S.A., Institute of Electrical and Electronics Engineers (IEEE). pp. 17-21. doi: 10.1109/ICMRE49073.2020.9065011.

Ben Jabeur, C. & Seddik, H. (2021) Design of a PID optimized neural networks and PD fuzzy logic controllers for a two-wheeled mobile robot. *Asian Journal of Control.* 23(1), 23–41. doi: 10.1002/asjc.2356.

Blasko, V. & Kaura, V. (1997) A new mathematical model and control of a three-phase AC-DC voltage source converter. *IEEE Transactions on Power Electronics.* 12(1), 116–123. doi: 10.1109/63.554176.

Coteli, R., Acikgoz, H., Ucar, F. & Dandil, B. (2017) Design and implementation of Type-2 fuzzy neural system controller for PWM rectifiers. *International Journal of Hydrogen Energy.* 42(32), 20759–20771. doi: 10.1016/j.ijhydene.2017.07.032.

Dian, S., Han, J., Guo, R., Li, S., Zhao, T., Hu, Y. & Wu, Q. (2019) Double Closed-Loop General Type-2 Fuzzy Sliding Model Control for Trajectory Tracking of Wheeled Mobile Robots. *International Journal of Fuzzy Systems.* 21(7), 2032–2042. doi: 10.1007/ s40815-019-00685-z.

Dong, H. & Luo, Z. (2011) Control Strategies of Human Interactive Robot Under Uncertain Environments. In: Będkowski, J. (ed.) *Mobile Robots: Control Architectures, Bio-Interfacing, Navigation, Multi Robot Motion Planning and Operator Training.* Croatia, InTech, pp. 55-80. doi: 10.5772/2304.

Eltamaly, A. M., Alolah, A. I. & Badr, B. M. (2010) Fuzzy controller for three phases induction motor drives. In: *IEEE 2010 International Conference on Autonomous and Intelligent Systems (AIS 2010), 21-23 June 2010, Povoa de Varzim, Portugal.* New Jersey, U.S.A., Institute of Electrical and Electronics Engineers (IEEE). pp. 1-6. doi: 10.1109/AIS.2010.5547020.

Gholipour, A. & Yazdanpanah, M. J. (2003) Dynamic tracking control of nonholonomic mobile robot with model reference adaptation for uncertain parameters. In: *2003 European Control Conference, 01-04 September 2003, Cambridge, UK.* New Jersey, U.S.A., Institute of Electrical and Electronics Engineers (IEEE). pp. 3118–3122. doi: 10.23919/ECC.2003.7086518.

Huang, P., Zhang, Z., Luo, X., Zhang, J. & Huang, P. (2018) Path Tracking Control of a Differential-Drive Tracked Robot Based on Look-ahead Distance. *IFAC-PapersOnLine.* 51(17), 112-117. doi: 10.1016/j.ifacol.2018.08.072.

Jayakumar, V. & Kumar, M. (2012) *Engineering Mechanics.* New Delhi, India, PHI Learning Private Limited, pp. 100-123.

Ji, P., Li, S., Xu, M., Li, J. & Guo, J. (2018) Design of Sliding Cloud-Model Cross Coupling Controller for Tracked Mobile Robot. In: *2018 37th Chinese Control Conference (CCC), 25-27 July 2018, Wuhan, China.* New York City, U.S.A., Institute of Electrical and Electronics Engineers (IEEE). pp. 5353–5357. doi: 10.23919/ChiCC.2018.8483174.

Karnik, N. N. & Mendel, J. M. (1998) Type-2 fuzzy logic systems: type-reduction. In: *1998 IEEE International Conference on Systems, Man, and Cybernetics (SMC'98), 14 October 1998, San Diego, CA, U.S.A.* New Jersey, U.S.A, Institute of Electrical and Electronics Engineers (IEEE). pp. 2046-2051. doi: 10.1109/ICSMC.1998.728199.

Kayacan, E. & Khanesar, M. A. (2015) *Fuzzy Neural Networks for Real Time Control Applications: Concepts, Modeling and Algorithms for Fast Learning.* Oxford, United Kingdom, Butterworth-Heinemann.

Kececioglu, O. F. (2022) Design of type-2 fuzzy logic controller optimized with firefly algorithm for maximum power point tracking of photovoltaic system based on super lift Luo converter. *International Journal of Numerical Modelling: Electronic Networks, Devices and Fields.* 35(4), e2994. doi: 10.1002/jnm.2994.

Kececioglu, O. F., Gani, A., Kilic, E. & Sekkeli, M. (2019) Dynamic Performance Evaluation of PI and Interval Type-2 Takagi-Sugeno-Kang Fuzzy Controller on Positive Output Luo Converter. *Natural and Engineering Sciences.* 4(3), 32–39.

Kılıc, E., Ozcalık, H.R. & Sit, S. (2018) Adaptive controller with RBF neural network for induction motor drive. *International Journal of Numerical Modelling Electronic Networks Devices and Fields.* 31(3), 1–11. doi: 10.1002/jnm.2280.

Liang, Q. & Mendel, J. M. (2000) Interval type-2 fuzzy logic systems: theory and design. *IEEE Transactions on Fuzzy Systems.* 8(5), 535-550. doi: 10.1109/91.873577.

Lin, T.-C., Chen, C.-C. & Lin, C.-J. (2020) Using Interval Type-2 Recurrent Fuzzy Cerebellar Model Articulation Controller Based on Improved Differential Evolution for Cooperative Carrying Controller of Mobile Robots. In: *2020 International Conference on Fuzzy Theory and Its Applications, 04-07 November 2020, Hsinchu, Taiwan.* New Jersey, U.S.A., Institute of Electrical and Electronics Engineers (IEEE). pp. 1-3. doi: 10.1109/iFUZZY50310.2020.9297367.

Mallick, A. K. & Das, A. (2023) Design of an Improved Interval Type-2 Controller Using FCM and Supervised Clustering Algorithms. *Studies in Informatics and Control.* 32(3), 89-98. doi: 10.24846/v32i3y202308.

Malu, S. K., & Majumdar, J. (2014) Kinematics, Localization and Control of Differential Drive Mobile Robot. *Global Journal of Researches in Engineering: Robotics & Nano-Tech.* 14(1), 1-9.

Mendel, J. & John, R. (2002) Type-2 fuzzy sets made simple. *IEEE Transactions on Fuzzy Systems*. 10(2), 117-127. doi: 10.1109/91.995115.

Najmurrokhman, A., Komarudin, U., Djamal E. C. & Taufik F. (2019) Speed Control and Obstacle Avoidance of a Hexapod Mobile Robot using Mamdani type Fuzzy Logic Controller. In: *6th International Conference on Instrumentation, Control, and Automation (ICA), 31 July - 2 August 2019, Bandung, Indonesia.* New Jersey, U.S.A., Institute of Electrical and Electronics Engineers (IEEE). pp. 199-202. doi: 10.1109/ICA.2019.8916714.

Peng, H., Wang, J., Wang, S., Shen, W., Shi D. & Liu, D. (2020) Coordinated Motion Control for a Wheel-Leg Robot With Speed Consensus Strategy. *IEEE/ASME Transactions on Mechatronics.* 25(3), 1366-1376. doi: 10.1109/TMECH.2020.2975083.

Pour, P. D., Alsayegh, K. M. J. & Jaradat, M. A. (2022) Type-2 Fuzzy Adaptive PID Controller for Differential Drive Mobile Robot: A Mechatronics Approach. In:

Advances in Science and Engineering Technology International Conferences (ASET), 21-24 February 2022, Dubai, United Arab Emirates. New Jersey, U.S.A., Institute of Electrical and Electronics Engineers (IEEE). pp. 1-6. doi: 10.1109/ASET53988.2022.9734882.

Serway, R. A., Jewett, J. W., Wilson, K. & Rowlands, W. (2016) *Physics for Global Scientists and Engineers*. Volume 2. 2nd ed. New Zeeland, Australia, Cengage Learning.

Sidi, M. H. A., Hudha, K., Kadir, Z. A. & Amer, N. H. (2018) Modeling and path tracking control of a tracked mobile robot. In: *IEEE 14th International Colloquium on Signal Processing and its Application, 09-10 March 2018, Penang, Malaysia.* New Jersey, U.S.A., Institute of Electrical and Electronics Engineers (IEEE). pp. 72–76. doi: 10.1109/CSPA.2018.8368688.

Sun, H., Chen, Y.-H., Huang, K. & Qiu, M. (2019) Controlling the differential mobile robot with system uncertainty: Constraint-following and the adaptive robust method. *Journal of Vibration and Control.* 25(6), 1294-1305. doi: 10.1177/1077546318821166.

Takagi, T. & Sugeno, M. (1985) Fuzzy identification of systems and its applications to modeling and control. *IEEE Transactions on Systems, Man, and Cybernetics*. SMC-15(1), 116-132. doi: 10.1109/TSMC.1985.6313399.

Tavoosi, J., Suratgar, A. A., Menhaj, M. B., Mosavi, A., Mohammadzadeh, A. & Ranjbar, E. (2021) Modeling renewable energy systems by a self-evolving nonlinear consequent part recurrent type-2 fuzzy system for power prediction. *Sustainability.* 13(6), 3301. doi: 10.3390/su13063301.

Vidlak, M., Makys, P. & Stano, M. (2021) Comparison between model based and non-model based sensorless methods of brushed DC motor. *Transportation Research Procedia*. 55, 911-918. doi: 10.1016/j.trpro.2021.07.059.

Wu, D. (2012) Twelve considerations in choosing between Gaussian and trapezoidal membership functions in interval type-2 fuzzy logic controllers. In: *IEEE International Conference on Fuzzy Systems, 10-15 June 2012, Brisbane, QLD, Australia.* New Jersey, U.S.A., Institute of Electrical and Electronics Engineers (IEEE). pp. 1-8. doi: 10.1109/FUZZ-IEEE.2012.6251210.

Wu, X., Xu, M. & Wang, L. (2013) Differential speed steering control for four-wheel independent driving electric vehicle. In: *IEEE International Symposium on Industrial Electronics, 28-31 May 2013, Taipei, Taiwan.* New Jersey, U.S.A., Institute of Electrical and Electronics Engineers (IEEE). pp. 1-6. doi: 10.1109/ISIE.2013.6563667.

Ye, B., Yao, X. & Yang, Y. (2016) Speed Control of Mobile Robot Based on LADCR. In: *8th International Conference on Intelligent Human-Machine Systems and Cybernetics (IHMSC), 27-28 August 2016, Hangzhou, China.* New Jersey, U.S.A., Institute of Electrical and Electronics Engineers (IEEE). pp. 310-313. doi: 10.1109/IHMSC.2016.88.

Zadeh, L. A. (1975) The concept of a linguistic variable and its application to approximate reasoning-I. *Information Sciences.* 8(3), 199–249. doi: 10.1016/0020-0255(75)90036-5.